Zeolite beta doped with La, Fe, and Pd as a hydrocarbon trap

catalysts

MDPI

Article

Zeolite Beta Doped with La, Fe, and Pd as a Hydrocarbon Trap

Rasmus Jonsson, Jungwon Woo, Magnus Skoglundh and Louise Olsson *

Competence Centre for Catalysis, Chalmers University of Technology, SE-412 96 Gothenburg, Sweden; rasjon@chalmers.se (R.J.); jungwon@chalmers.se (J.W.); skoglund@chalmers.se (M.S.)

* Correspondence: louise.olsson@chalmers.se; Tel.: +46-31-772-4390

Received: 20 December 2019; Accepted: 26 January 2020; Published: 2 February 2020

Abstract: Hydrocarbon trapping is a technique of great relevance, since a substantial part of hydrocarbon emissions from engines are released from engines before the catalyst has reached the temperature for efficient conversion of the hydrocarbons. In this work, the influence of doping zeolite beta (BEA) with Fe, Pd, and La on the storage and release of propene and toluene is studied. Five monolith samples were prepared; Fe/BEA, La/BEA, Pd/BEA, Pd/Fe/BEA, and Pd/La/BEA using incipient wetness impregnation, and the corresponding powder samples were used for catalyst characterization by Inductively coupled plasma sector field mass spectrometry (ICP-SFMS), Temperature-programmed oxidation (TPO), X-ray photoelectron spectroscopy (XPS) and Scanning transmission electron microscopy with Energy dispersive X-ray analysis (STEM-EDX). The hydrocarbon trapping ability of the samples was quantified using Temperature-programmed desorption (TPD) of propene and toluene, and in situ Diffuse reflectance infrared Fourier transform spectroscopy (DRIFTS). The results from the TPD experiments show that the addition of Pd and La to the zeolite affected the release patterns of the stored hydrocarbons on the trapping material in a positive way. The in situ DRIFTS results indicate that these elements provide H-BEA with additional sites for the storage of hydrocarbons. Furthermore, EDX-mapping showed that the La and Pd are located in close connection.

Keywords: HC trap; cold-start; toluene; zeolite; Pd-BEA; Fe-BEA

1. Introduction

Exhaust aftertreatment is crucial to reduce emissions from large fleets of vehicles all over the world. For gasoline vehicles, the three-way-catalyst (TWC) concept is applied for the removal of hydrocarbons (HC), and for diesel vehicles, lean NOx traps (LNT) or diesel oxidation catalysts (DOC) are applied. While these catalysts function well after the so called 'light-off' temperature has been reached, none of them can remove unwanted hydrocarbons (HC), carbon monoxide (CO), and nitrogen oxides (NOx) from the exhausts during the heating of the catalyst from the cold-start of the engine. This results in that 80%–90% of the pollutants are emitted during the cold-start [1–4]. It is, therefore, desirable to trap NOx and HC [5] at low temperature and release these components when the catalyst system is above the light-off temperature and able to efficiently convert them to N_2, CO_2, and H_2O.

HC traps usually consist of zeolites [6–9], and the hydrocarbons desorbs from the trap around 200–250 °C [5]. The desorption temperature depends on the size and polarity of the hydrocarbon [10–12], as well as its interaction with the zeolite [13,14]. Two of the more commonly studied compounds for HC traps are toluene and propene [14–16]. These two compounds interact with the zeolite in different ways. It has been proposed that propene primarily interacts with the Brønsted acid sites through hydrogen bonding with the pi electrons in the C=C bond, which makes trapping of propene beneficial for low Si/Al ratios of the zeolite [17]. Toluene; however, is proposed to interact with both the Brønsted

and Lewis acid sites. Negatively charged oxygen in the zeolite structure interacts with the methyl group in toluene, while the Lewis and Brønsted acid sites interact with the phenyl ring [10–12,18–20].

Burke et al. [21] have studied the effect of hydrothermal aging of La-exchanged zeolite beta. The authors found that after thermal treatment, the adsorption of propene decreases considerably, whereas the adsorption of toluene increases. This finding indicates that dealumination decreases the amount of Brønsted acid sites, thus making the zeolite more hydrophobic, which then governs the adsorption of toluene in the zeolite, but suppresses the adsorption of propene [21].

With a low Si/Al ratio, the zeolite becomes more hydrophilic due to an increase in the number of Brønsted acid sites. This property is desired since it enhances the trapping of smaller hydrocarbons. However, it also contributes to the trapping of water from the exhaust gas. Water has been proven to inhibit the trapping of hydrocarbons in exhaust gases due to strong interaction between water and the Brønsted acid sites [22,23].

One of the more common ways of enhancing the HC-trap system is to incorporate a metal cation into the porous structure of the zeolite. This is for the purpose of introducing more Lewis acid sites into the zeolite, thereby affecting the trapping pattern of the zeolite. One of the metals that has been extensively studied for this purpose is silver. Silver ion has been proven to provide good resistance to water while strongly binding hydrocarbons. This has been attributed to its size and the ionic charge of Ag^+ [23,24]. Another cation that has been extensively studied is Na^+ [10,25–27]. The trapping capacity of Na^+ has been attributed to its balance between Lewis acidity and basicity. This was concluded when Na^+ was compared to Li^+, K^+, and Cs^+ ions in a study by Takamitsu et al. [25]. The size of Na^+ was also found to be important for its trapping ability. Larger HC molecules occupy more space inside the zeolite channels, and due to this, small cations have an advantage over larger cations in this application [25]. Kobatake et al. have studied toluene trapping in Fe-exchanged zeolite beta. Their findings indicate that the incorporation of iron to the zeolite contributes to cracking and oxidation of toluene to CO_2 during cold-starts [28].

Incorporating Pd into the zeolite has been found to enhance the trapping ability and conversion of stored hydrocarbons in zeolites. Xu et al. have studied the HC-trapping capability of Pd/BEA in an E85 fuel-based emission control system. The authors found that Pd contributes to the reaction mechanism by providing paths for dehydration and decomposition of the hydrocarbons, which results in a reduction of the release of hydrocarbons to the exhausts [29]. Moreover, the addition of Pd together with other redox active metals to HC trap systems has been proven to be beneficial also for emissions from gasoline-based fuels. This was observed by Lupescu et al. as they studied direct-injected gasoline into the exhaust aftertreatment system of a Ford Focus passenger car. They found that the Brønsted acid sites, Pd, and redox-active metals allow the polymerisation of stored HC compounds and that the base redox metal also helps stabilize the Pd from sintering [30].

However, to our knowledge, no studies are available in the open literature that compare and evaluate the effect of promoting zeolite beta with Pd, La, and Fe used as a hydrocarbon trap, which is the objective of the present study.

2. Results and Discussion

2.1. Catalyst Characterisation

The elemental composition of the samples was measured using inductively coupled plasma-sector field mass spectroscopy (ICP-SFMS), and the results are shown in Table 1, performed by ALS Scandinavia.

Table 1. ICP-SFMS results for the prepared powder samples.

	Fe/BEA	Pd/Fe/BEA	Pd/BEA	Pd/La/BEA	La/BEA
Fe (wt-%)	1.1	1.1	-	-	-
La (wt-%)	-	-	-	2.6	2.6
Pd (wt-%)	-	1.9	2.1	1.9	-
SiO_2/Al_2O_3	21.7	23.6	22.3	22.1	23
Pd/Al_2	-	0.31	0.34	0.33	-

Freshly calcined catalyst powder was subjected to temperature-programmed oxidation (TPO) to study the impact Fe and La might have on the oxidation of Pd. The results from the TPO experiments are shown in Figure 1. The results in the figure shows that Pd/BEA has a distinct temperature of oxidation centered at 330 °C, which has been confirmed by other studies of BEA impregnated with Pd [31]. The major peak of oxidation for Fe/BEA was found at 230 °C; however, this peak is considerably lower magnitude than the peak associated with the Pd-containing samples. The La/BEA sample shows only a minor peak at high temperature. These results show that the main oxygen consumption in the Pd-containing samples originates from the Pd. Interestingly, a shift towards a higher temperature of oxidation was found for the Pd/Fe/BEA and Pd/La/BEA samples, to 345 and 385 °C, respectively. In addition, two small oxidation peaks are also visible at 130 and 318 °C for Pd/Fe/BEA. The results show that the addition of Fe and La to Pd/BEA results in higher activation energy for the oxidation of most Pd, but that there also is some Pd that is easily oxidized for Pd/Fe/BEA. The TPO data show that there are clear interactions between Fe and Pd, and between La and Pd. Moreover, the two smaller peaks at 130 and 318 °C for Pd/Fe/BEA, could originate from the oxidation of iron, since a peak at 230 °C was visible for Fe/BEA, which was not the case for Pd/Fe/BEA. These results indicate that not only Pd is influenced by Fe, but also that the oxidation of Fe is affected by the presence of Pd. The magnitude of the oxidation peaks for the promoted samples is almost halved, compared to the pure Pd/BEA sample. We hypothesize that the reason for this could be that Fe or La blocks access to some of the Pd sites due to steric hindrance.

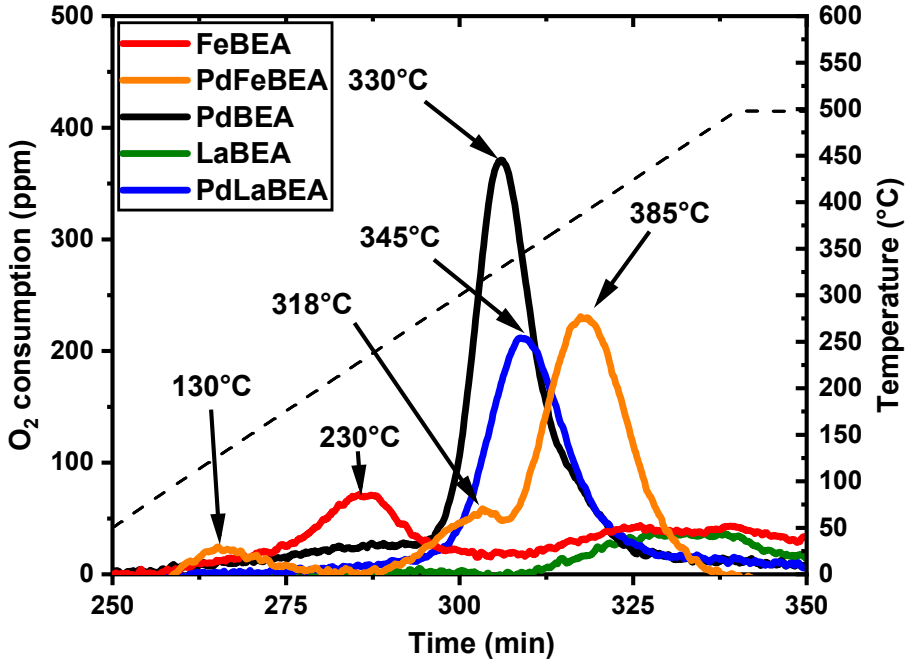

Figure 1. Oxygen consumption for the samples (solid lines) during temperature-programmed oxidation plotted versus time. The corresponding temperature profile (dashed line) is also given.

In addition to the TPO, fresh calcined powder samples were analyzed by XPS to determine the oxidation state of Pd in the presence of La and Fe, and the results are shown in Figure 2. It should be noted that due to the low atomic percentage of the Pd, there are uncertainties in the data. The spectra for all samples were shifted based on both the Si 2p (103.6 eV) and Al 2P (74.8 eV) due to the large amount of these elements in the zeolite beta framework. The shift observed for the Pd 3d5/2 peak indicates that the addition of Fe and La affects the Pd, when compared to the Pd/BEA sample. At higher binding energies, the Pd is more oxidized, this indicates that impregnation of Fe and La results in a lower oxidation state of Pd.

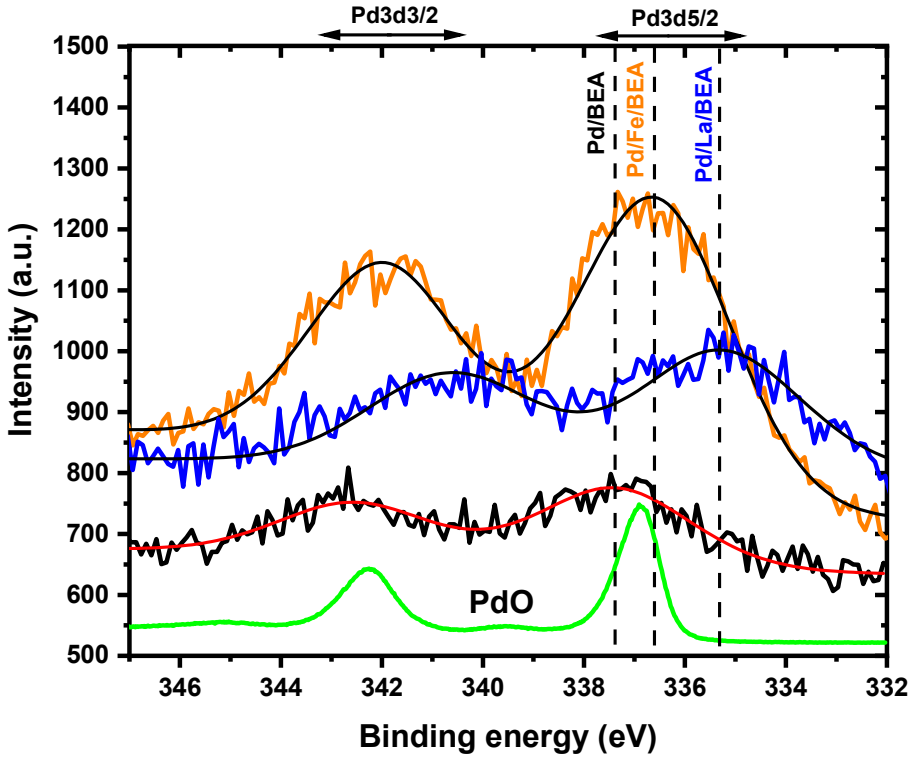

Figure 2. XPS measurements over Pd 3d3/2 and Pd 3d5/2. Pd/BEA in black, Pd/Fe/BEA in orange and Pd/La/BEA in blue. Dashed lines mark peak centers for Pd 3d5/2.

Scanning transmission electron microscopy energy-dispersive X-ray (STEM-EDX) analysis was performed on freshly calcined powder samples of Pd/Fe/BEA and Pd/La/BEA. The results are shown in Figure 3. Images were collected over areas containing agglomerates of Pd. The first row contains images from Pd/Fe/BEA, and the second row from Pd/La/BEA. Silicon, aluminum, and oxygen are evenly distributed and follow a similar pattern. This was expected since these elements originate from the zeolite framework structure. Iron was detected in connection to Pd for Pd/Fe/BEA; however, iron was also detected in other locations. It can be seen in the figure that La and Pd are located closer to each other than Fe and Pd. It is important to note that for zeolites functionalized using incipient wetness impregnation, most Pd, Fe, and La are likely present inside the porous zeolite structure. However, STEM-EDX accessed mainly particles on the outside of the zeolite crystals with the resolution of the STEM-EDX in the figure due to the size-limitation on particles in the porous structure of the zeolite. However, the results from the STEM-EDX analysis nicely correlate with the results from the TPO measurements (Figure 1), where both La and Fe were found to influence the oxidation temperature of Pd, thus indicating a clear interaction with Fe/La and Pd.

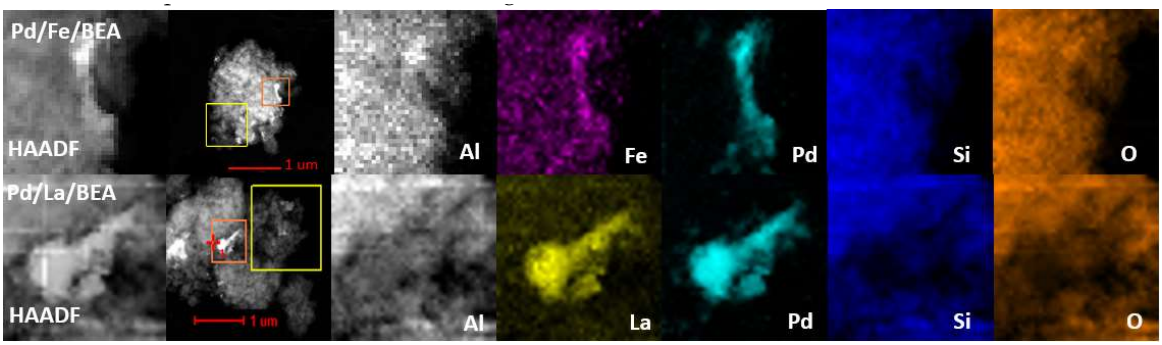

Figure 3. Transmission electron microscopy (TEM) and energy-dispersive X-ray (EDX) mapping of the samples: Pd/Fe/BEA (top row) and Pd/La/BEA (bottom row).

2.2. Temperature-Programmed Desorption of Hydrocarbons

Temperature-programmed desorption (TPD) of propene was performed in dry conditions to evaluate the adsorption and desorption of smaller hydrocarbons. The results are shown in Figure 4. Panel A contains the desorption profiles for BEA, Fe/BEA, La/BEA, and Pd/BEA, and Panel B contains the profiles from the samples where Pd and Fe, or La together with Pd are present (Pd/BEA, Pd/Fe/BEA and Pd/La/BEA). The results show that the desorption maximum of propene is primarily located around 250 °C for all samples, including the BEA reference sample. This indicates that the desorption of propene in this temperature range can be associated with desorption from the zeolite BEA, i.e., the Brønstedt acid sites [5,17]. The high storage capacity of propene in Figure 4 can be explained by the low SiO_2/Al_2O_3 ratio of the zeolite used in the present study, which is consistent with previous studies [17,18,25]. Furthermore, the XPS results (see Figure 2) show that the oxidation state of Pd becomes lower when introducing Fe and especially La. The same trend is found for the propene TPD, where Pd/Fe/BEA, and especially Pd/La/BEA, desorb higher amounts of propene, indicating that a lower oxidation state of Pd is beneficial for the storage of propene.

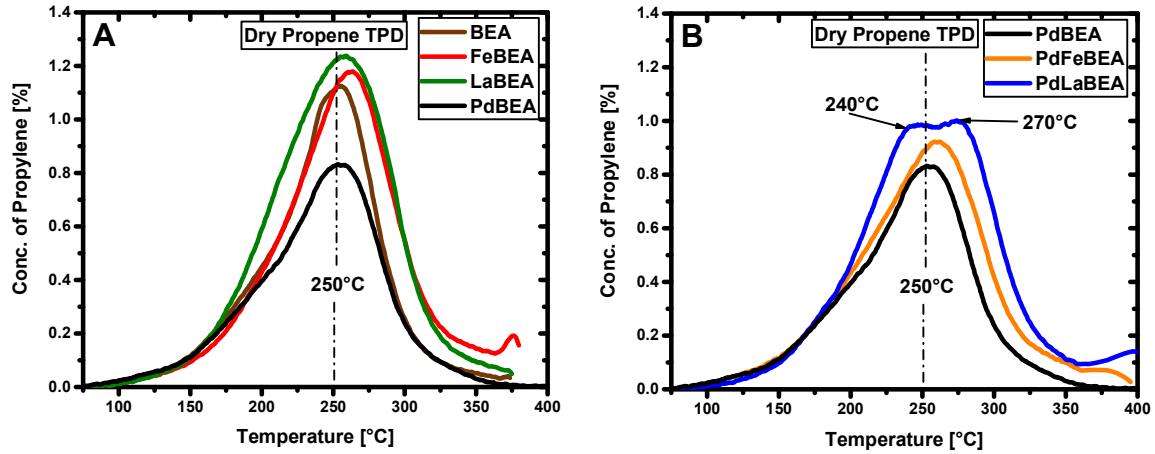

Figure 4. Temperature-programmed desorption (TPD) of propene at dry conditions where the concentration of propene is plotted against the corresponding desorption temperature during the heating ramp. The samples were pre-oxidized at 400 °C. The desorption profiles for (**A**) BEA, Fe/BEA, La/BEA and Pd/BEA; and for (**B**) Pd/BEA, Pd/Fe/BEA and Pd/La/BEA are shown.

After the propene TPD, the sample was oxidized using 10% O_2 at 400 °C for 20 min. The formed CO and CO_2 show that some residual carbon remained on the surface after the TPD. The distribution of C_3H_6, CO, and CO_2 during desorption is shown in Table 2, where the components are translated into C1-eqvivalents.

Table 2. Distribution of the C1-equivavlents that account for the C_3H_6 desorption as well as the CO and CO_2 production during the oxidation step following the propene-TPD in Figure 1. The data is given in % distribution of how the carbon leaves the samples.

	BEA	FeBEA	LaBEA	PdBEA	PdFeBEA	PdLaBEA
CO (%)	0.63	0.55	1.56	0.11	0.07	0.33
CO_2 (%)	1.07	2.52	3.15	4.19	2.42	2.68
C_3H_6 (%)	98.3	96.9	95.3	95.9	97.5	70.0

The Pd/BEA and La/BEA samples produced a larger fraction of CO and CO_2 during the oxidative regeneration after the TPD than the other samples, of which, BEA produced the least. These results suggest that Pd and La can store some hydrocarbon species with high binding strength compared to the BEA sample. However, the CO and CO_2 production was low compared with the desorption of C_3H_6 for all samples. It can also be seen in Figure 4 that the samples containing Pd desorbed less than the other samples. These samples produce more CO and CO_2 than the pure BEA sample; however, the formation of CO_x ($CO+CO_2$) is low (2%–4% of total C1 species) and it is therefore clear that there was significantly less propene stored on these samples. A possible reason for this finding is that the added Pd partially blocks the Brønstedt acid sites that are active in storing hydrocarbons in dry conditions.

Propene-TPD experiments performed in wet conditions (5% H_2O) were conducted; however, the results did not indicate any propene storage. This is most likely due to the competition of water and propene for the hydrophilic sites in the zeolite structure [22,32].

Since toluene is a major component of gasoline, it is highly relevant when studying HC-trap mechanisms. Toluene-TPD experiments were consequently performed. The results for toluene-TPD experiments performed in dry conditions are shown in Figure 5. For all samples, a large desorption peak ranging from 100 to 180 °C can be seen. This peak is attributed to storage of toluene in the zeolite [24]. In this temperature region, it can also be seen that the desorption of toluene is highest for Pd/BEA and lowest for Fe/BEA. The addition of La and Pd, in particular, clearly improves the storage capacity of toluene compared to the pure zeolite beta sample. These results contradict the results from the propene-TPD experiments, where the addition of Pd resulted in lower storage capacity of propene in dry conditions. We suggest that the reason for this difference is that the phenyl ring of toluene can also adsorb Lewis acid sites [10–12,18–20], such as Pd, while propene preferentially interacts with Brønsted acid sites through hydrogen bonding with the π electrons in the C=C bond [17]. Some desorption peaks also appear at higher temperatures in Figure 5. The BEA reference sample only desorbed minor amounts of toluene at higher temperatures, which was also found for Fe/BEA and Pd/BEA. Interestingly, the La/BEA sample has a desorption peak at 240 °C, which increases in the presence of Pd (see the Pd/La/BEA sample in Figure 5B), despite that the Pd/BEA sample exhibits no desorption peak in this region. These results show that there is clear interaction between the La and Pd, which was also concluded from the TPO experiments in which a clear shift of the oxidation temperature of Pd was found when La was added to Pd/BEA.

The ethene produced during the toluene-TPD experiments performed in dry conditions is shown in Figure 6. It is clear from the figure that toluene undergoes significant cracking in the porous structure of the zeolite beta. Ethene was found to be the most common component from the cracking of toluene in these experiments. The ethene desorption peak is centered between 235 and 270 °C, which is close to the temperature range of the desorption of propene, as shown in Figure 4. This result indicates that toluene cracks into smaller components, which adsorb on the Brønsted acidic sites in the porous structure of the zeolite. The pure BEA sample cracked the toluene molecules to a much higher degree than the zeolite samples functionalized with Fe, La, and Pd. It is well known that zeolites are used in refinery operations for catalytic cracking, which occurs on Brønsted acid sites [33].

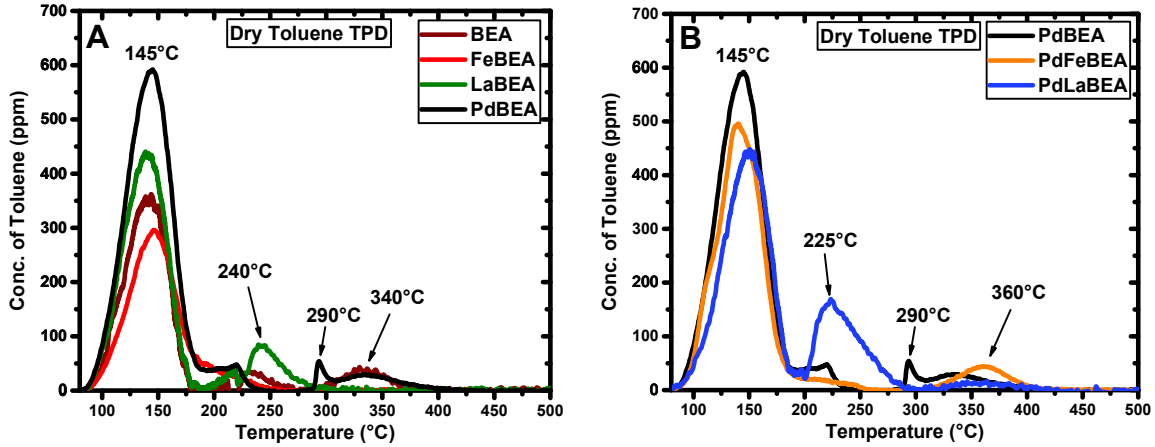

Figure 5. Temperature-programmed desorption of toluene in dry conditions where the concentration of toluene is plotted against the corresponding desorption temperature during the heating ramp for (**A**) BEA, Fe/BEA, La/BEA, and Pd/BEA; and for (**B**) Pd/BEA, Pd/Fe/BEA, and Pd/La/BEA.

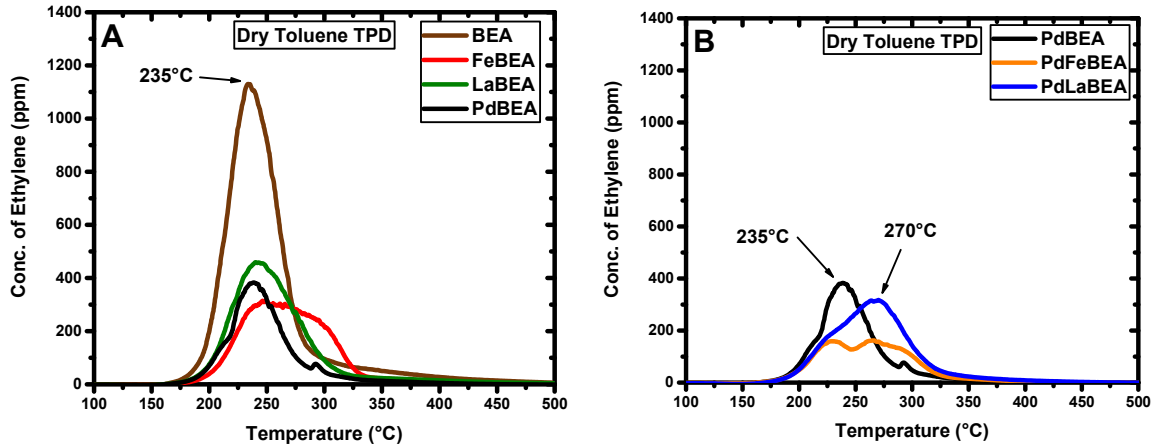

Figure 6. Temperature-programmed desorption of toluene in dry conditions where the concentration of formed ethene is plotted against the corresponding temperature for (**A**) BEA, Fe/BEA, La/BEA, and Pd/BEA; and (**B**) Pd/BEA, Pd/Fe/BEA, and Pd/La/BEA.

During cold-starts, ethene is present in high concentrations, fairly equal to the aromatic compounds in the exhaust, such as toluene, when normalized to C1 [34]. Westermann et al. [35] have studied the adsorption and desorption of mixed hydrocarbons for different zeolites. For H-BEA (SiO_2/Al_2O_3 ratio of 25), they observed desorption of toluene with a main peak in the same temperature region as found in the present study (Figure 5) with shoulders of toluene desorbing around 300 °C. For propene, the authors observed desorption centered at 290 °C [35], which is similar to our results in Figure 4 with a desorption peak at 250 °C. Moreover, Westermann et al. [35] observed relatively weak desorption of ethene starting above 200 °C from H-BEA (SiO_2/Al_2O_3-ratio of 25). However, for the other zeolites they studied (HY-15, HMOR-10, HZSM-5-5.5, HFER-10), the desorption of ethene always occurred above 200 °C, which agrees well with our results, as presented in Figure 6. In addition, minor amounts of CO were formed during the toluene-TPD experiments, except for the BEA reference sample (see Figure 7). This can be due to the presence of low amounts of oxygen from the degreening of the samples or from adsorbed water species that react with some of the adsorbed hydrocarbon species.

Temperature-programmed desorption of toluene in wet conditions was performed to investigate the capacity of the samples to store toluene in a more realistic environment, since water vapor is naturally formed during the combustion of hydrocarbon-based fuels. The wet toleune-TPD experiments were conducted similar to the corresponding experiments in dry conditions with the exception of the presence of 5% H_2O, both in the storage phase and during the following heating ramp. It is known

that the desorption patterns of adsorbed hydrocarbons are affected by the presence of water in the gas stream, which for example was found by Takamitsu et al. when studying the effect of different alkali metal ions on the adsorption of toluene [25]. Furthermore, Kang et al. have observed HC adsorption and desorption for Ag-BEA and they found that water inhibits the adsorption and desorption of hydrocarbons. Smaller hydrocarbons have been found to be more affected by the presence of water than larger hydrocarbon chains [24]. The results from the toluene-TPD experiments in wet conditions are shown in Figures 8–10, where the concentration of toluene is shown in Figure 8. It was found that the samples containing Pd desorbed a larger quantity of toluene. This trend is similar to the dry toluene-TPD experiments. A similar amount of toluene was found to desorb in both dry and wet conditions. These results indicate that toluene adsorbs on sites that are not affected to a large extent by water in the feed, or that the toluene adsorption is so strong that it can compete with the water. These results are interesting and are the exact opposite of the corresponding findings for propene adsorption, where water completely blocks the adsorption capacity of the hydrocarbon. The results suggest that the Lewis acid storage sites are less affected by the presence of water since propene mainly adsorbs on Brønsted acid sites [17], whereas toluene can adsorb on Lewis acid sites [10–12,18–20].

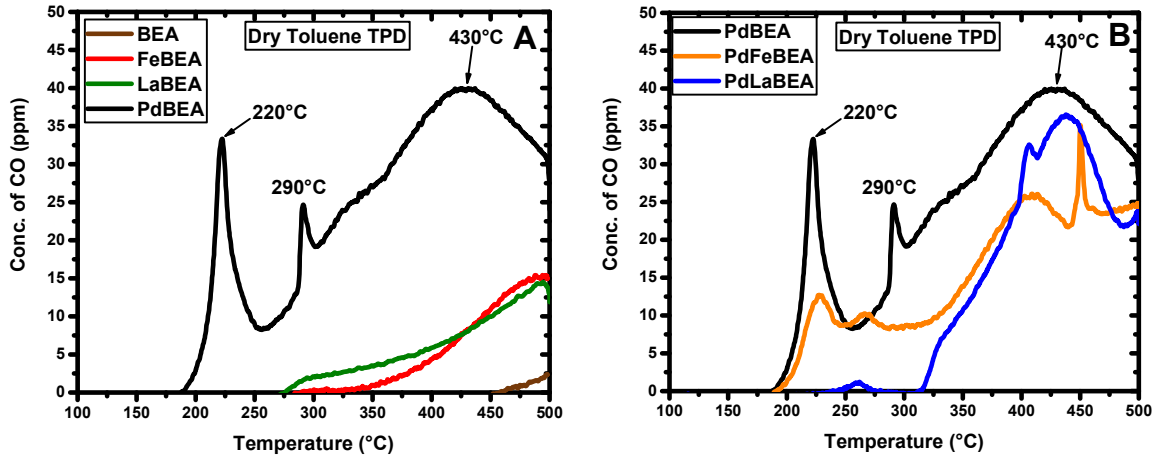

Figure 7. Temperature-programmed desorption of toluene in dry conditions where the concentration of formed CO is plotted against the corresponding temperature for (**A**) BEA, Fe/BEA, La/BEA, and Pd/BEA; and (**B**) Pd/BEA, Pd/Fe/BEA, and Pd/La/BEA.

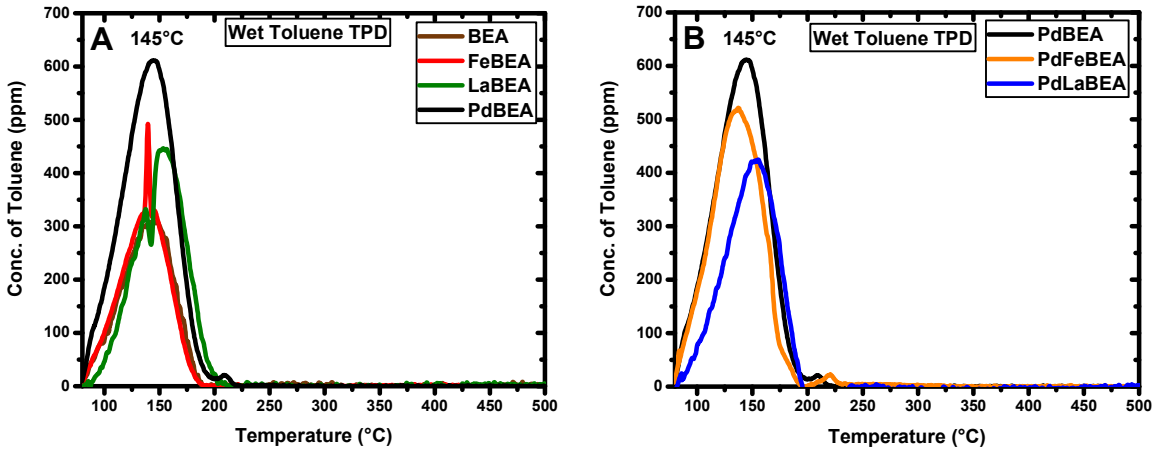

Figure 8. Temperature-programmed desorption of toluene in wet conditions where the concentration of toluene is plotted against the corresponding desorption temperature for (**A**) BEA, Fe/BEA, La/BEA, and Pd/BEA; and (**B**) Pd/BEA, Pd/Fe/BEA, and Pd/La/BEA.

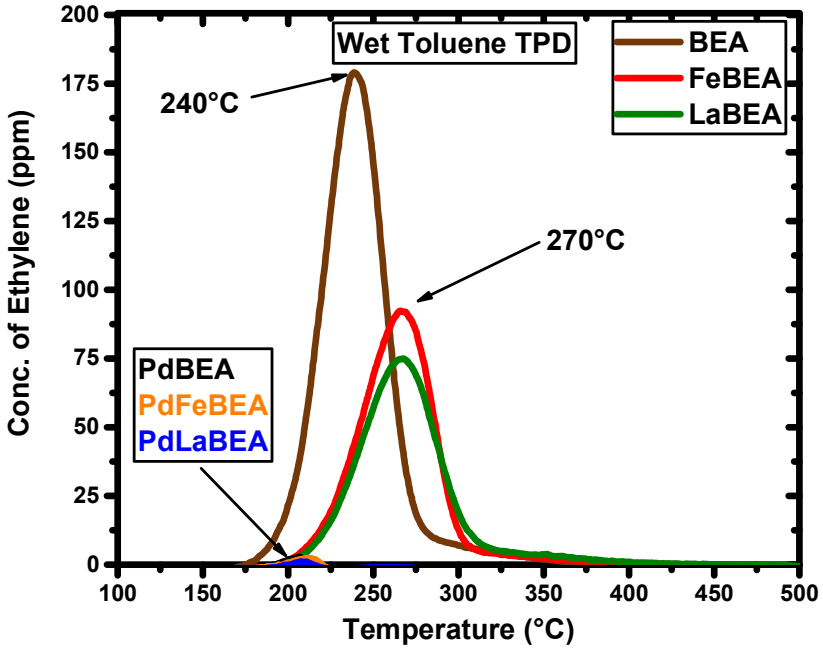

Figure 9. Temperature-programmed desorption of toluene at wet conditions where the concentration of formed ethene is plotted against the corresponding temperature for BEA, Fe/BEA, La/BEA, Pd/BEA, Pd/BEA, Pd/Fe/BEA, and Pd/La/BEA.

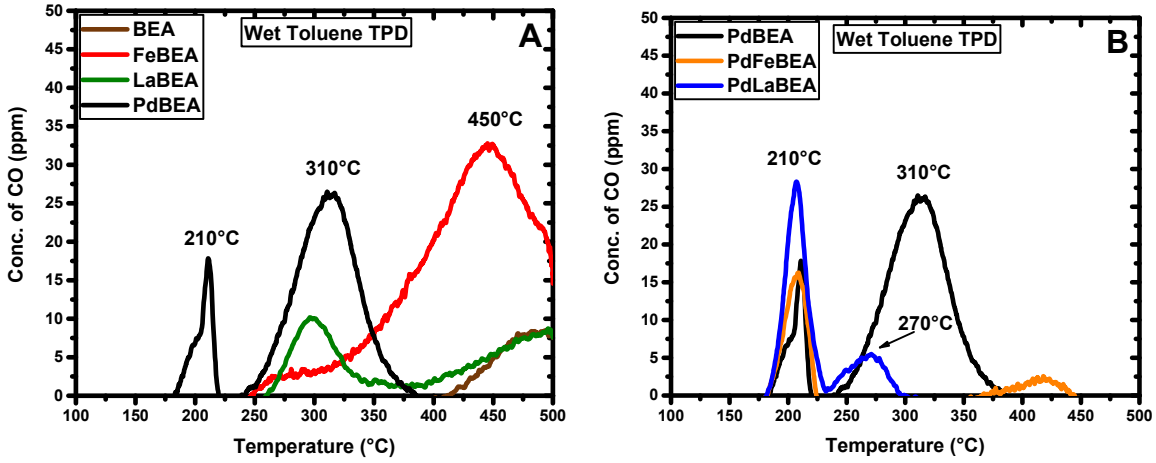

Figure 10. Temperature-programmed desorption of toluene at wet conditions where the concentration of formed CO is plotted against the corresponding temperature for (**A**) BEA, Fe/BEA, La/BEA, and Pd/BEA; and (**B**) Pd/BEA, Pd/Fe/BEA, and Pd/La/BEA.

Moreover, the results in Figure 8 show that adding Fe, and especially La to Pd/BEA, results in lowering of the amount of desorbed toluene. The XPS results (see Figure 2) show that the addition of Fe, and especially La, resulted in lowering of the Pd oxidation state. As the oxygen in the zeolite framework is mostly associated with Lewis acid sites [10–12,18–20]. The lower oxidation state of the Pd might indicate a lower number of Lewis acid sites, which could be an explanation for the lower desorption quantities observed in the toluene-TPD in Figure 8.

One significant difference between the dry and wet TPD experiments in the present study is in the higher temperature range, where no additional toluene desorption peaks exist when water is present in the feed.

When in the presence of water, some of the toluene cracks to ethene, which is shown in Figure 9. Compared to the dry toluene-TPD experiments, the quantity of ethene, which desorbed in the wet TPD experiments is considerably lower when water is introduced into the system. This can be explained by

water blocking the Brønsted acid sites, which are mainly responsible for the cracking. These results are consistent with the study on propene adsorption by Yoda et al. [17]. In that study, they found that propene adsorption occurs on Brønsted acid sites, which are blocked by the presence of water [17]. In Figure 9, the magnitude of the desorption peaks associated with Fe/BEA and La/BEA is about half that of a pure BEA sample; however, with a shift of about 30 °C from 240 to 270 °C. Moreover, the samples containing Pd barley desorb any ethene when water is present in the feed. It is known that there are significant interactions between Pd and water, which has been found in passive NOx adsorption studies, where the NO adsorption on Pd/zeolites is significantly reduced in the presence of water [31]. However, DRIFTS studies have shown that NO can replace some of the water species, causing water release [31]. Our findings suggest that toluene is very efficient in competing with water for Pd storage sites; however, the cracking of toluene does not seem to occur as it did in dry conditions.

Some CO is formed in the wet toluene-TPD experiments, as shown in Figure 10. The CO could originate from oxidation of adsorbed hydrocarbon species by remaining oxygen on the catalyst after the pre-treatment, or from steam-reforming reactions due to the presence of water in the feed. Several distinct peaks for CO appear in the figure, but the most dominant peaks are associated with either the zeolite samples functionalized with Pd or Fe/BEA. The amount of carbon desorbed in the form of CO is low in comparison with the desorption of toluene and ethene.

2.3. In Situ DRIFT Spectroscopy of Adsorbed Hydrocarbons during Heating

The adsorbed species on the samples were analyzed using *in situ* DRIFT spectroscopy during heating. Prior to the DRIFTS experiments, the samples were exposed to toluene in the same conditions as in the toluene-TPD experiments in the flow reactor system. The samples were first pre-oxidized and cooled in oxygen, and then exposed to 500 ppm toluene at 80 °C for 60 min, and finally, cooled to room temperature. Washcoat was scraped off from the monolith samples and then analyzed by DRIFTS. The IR spectrum from the pre-oxidized sample obtained after the toluene-TPD experiment at the same temperature was used as background and subtracted from the corresponding IR spectrum obtained during heating of the toluene exposed sample.

The DRIFTS results can be seen in Figure 11 for the temperatures 80, 150, 250, and 350 °C. The IR spectra recorded at the remaining temperatures can be found in the Supplementary information. Five negative absorption peaks were found in the high wavenumber region (4000–2000 cm^{-1}), which can be associated with the desorption of toluene. The absorption peaks located at 3088, 3063, and 3030 cm^{-1} are assigned to the C-H stretching vibrations of the aromatic ring of toluene. The peaks at 2920 and 2866 cm^{-1} are assigned to the asymmetric and symmetric C-H stretching vibrations of the methyl group [36,37]. These negative peaks were visible in samples containing Pd already at 80 °C, while the spectra for the other samples remained unchanged in this region until the temperature had increased above 100 °C. This indicates that the stability of stored toluene is slightly reduced in the presence of Pd.

In the low wavenumber region (2000–1000 cm^{-1}), the absorption peaks at 1602 and 1494 cm^{-1} are assigned to the in-plane skeletal vibrations of the aromatic ring, and the peak at 1294 cm^{-1} is assigned to symmetric C-C vibrations [38–40]. The DRIFTS spectra for all samples show a pronounced change at 150 °C, especially in the higher wavenumber region, which is located in the center of the toluene desorption peak observed in the TPD experiments, as shown in Figure 5. After the temperature had reached the desorption region of toluene, no further changes of the absorption peaks associated with toluene could be seen. These results indicate that the hydrocarbons remaining in the porous zeolite after the desorption temperature of toluene undergo some form of cracking.

The data presented in Figure 11 further indicate desorption of water from the surface of the samples. This can be seen by the broad negative band in the higher wavenumber region. The band starts at around 3600 cm^{-1} and continues to 2300 cm^{-1}. This region can be assigned to the stretching mode of H_2O [37]. We also found that the deformation mode of water at 1635 cm^{-1} was present in all samples [36,39]. Moreover, we also observe negative bands at 3682 cm^{-1} with increasing temperature,

which can be associated to O-H stretching vibrations of hydroxyl groups [41]. Before exposure to toluene, each sample was exposed to only dry conditions; however, in-between the exposure to toluene and the DRIFTS experiments, the samples were moved from the flow reactor to the DRIFT cell and were therefore exposed to air at room temperature, which can explain the presence of water. The spectra shown in Figure 11, further indicates that the adsorption sites in the zeolite framework are capable of adsorbing water even after 60 min of toluene exposure at 80 °C.

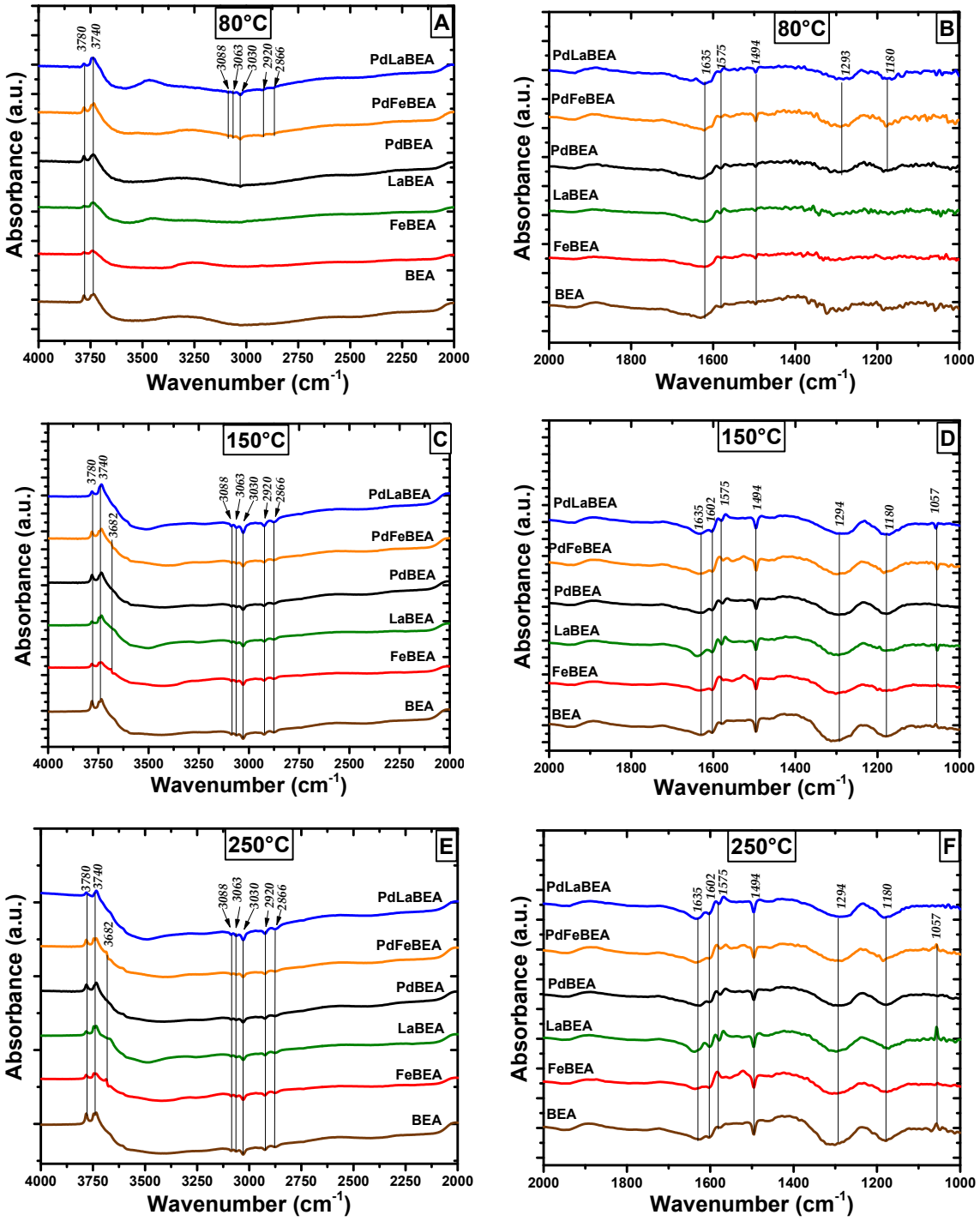

Figure 11. *Cont.*

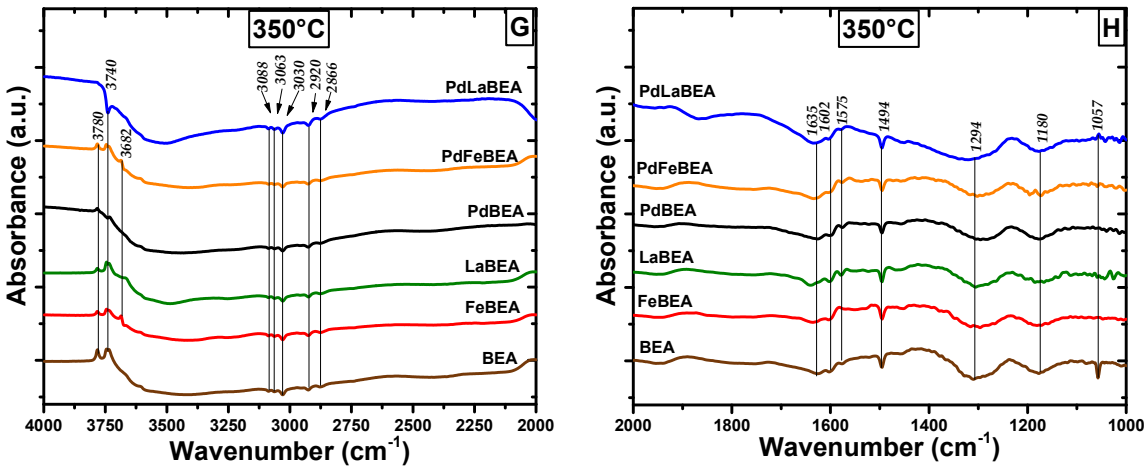

Figure 11. In situ DRIFTS spectra recorded in Ar after stepwise increasing the temperature from 80–350 °C after exposing the samples for toluene at 80 °C. Panels A, C, E, and G show the wavenumber region 4000–2000 cm^{-1}. Panels B, D, F, and H show the wavenumber region 2000–1000 cm^{-1}.

Already at 80 °C, we can observe positive absorption bands at 3780 and 3740 cm^{-1}, which are associated to hydroxyl groups. The peak located at 3740 cm^{-1} has previously been assigned to the O-H stretching of Si-OH groups, which has been observed for zeolite ZSM-5 [23]. Thus, the DRIFTS results suggest that some of the water species (2300–3600 cm^{-1}) are transformed to hydroxyl groups (at 3780 and 3740 cm^{-1}). Moreover, two peaks located around 1575 cm^{-1} can also be observed. These peaks appear to be similar for all samples, except for Fe/BEA and BEA, and are the strongest in the temperature range 200–250 °C. The main desorption of toluene had already occurred in this temperature range and the desorption occurred in the range where the desorption of ethene was observed in the samples in the toluene-TPD experiments (see Figure 6). It is, therefore, possible that these peaks are associated with cracking of toluene into smaller-sized hydrocarbon chains, which desorb. Given that pure zeolite beta and Fe/BEA do not provide any more absorption peaks in the region around 1575 cm^{-1}, while the other samples do, this may suggest that Pd and La provide the system with additional HC storage sites.

3. Materials and Methods

3.1. Sample Preparation

The five samples were prepared using incipient wetness impregnation of an H-BEA 25 (SiO_2/Al_2O_3 = 25, Zeolyst International) support with metal precursor solutions. Firstly, three batches containing 2 wt % of Pd and an equimolar amount of Fe and La were produced. A solution of the precursors ($Fe(NO_3)_3 \times 9H_2O$, $La(NO_3)_3$ $x5H_2O$, and palladium(II)nitrate) was prepared and mixed with the support material. The samples were then dried at 120 °C for 24 h, followed by calcination at 550 °C for 3 h with a heating ramp of 5 °C/min starting at room temperature. Half the batches containing Fe and La were then impregnated with the palladium precursor solution, dried at 120 °C for 24 h, and finally, calcined at 550 °C for 3 h.

The samples were then coated onto honeycomb-shaped cordierite substrates (400 cpsi, 21 mm in diameter and 20 mm in length). Parts of the sample batches were mixed with 5 wt % boehmite (Sasol Disperal P2) to improve the adhesiveness. The powder samples were mixed into a solution of 50 vol % deionized water, and 50 vol % ethanol was then coated onto the monolith substrates. The targeted washcoat amount on the monoliths was 700 mg, which corresponds to ca 100 g washcoat per L monolith. This was achieved using a stepwise procedure where the monolith was immersed into the prepared solution and then dried at 90 °C under a heating gun until the targeted amount was reached. Thereafter, the coated monolith samples were calcined at 550 °C for 2 h with a heating ramp of 5 °C/min starting from room temperature.

3.2. Catalyst Characterisation

All catalyst characterization was performed for freshly calcined powder samples.

The elemental composition of the samples was measured using ICP-SFMS, which was performed by ALS Scandinavia.

Temperature-programmed oxidation (TPO) was carried out by placing 100 mg of a powdered sample in a flow reactor. All samples were first reduced in 2 vol % H_2 at 500 °C for 30 min, then cooled to 100 °C in the presence of 2 vol % H_2. Subsequently, the reduced samples were exposed to 800 ppm O_2 at 100 °C for 3 h, which was followed by a heating ramp in 800 ppm O_2 from 100 to 500 °C with a heating rate of 10 °C per minute. The instrument used for the TPO was a differential scanning calorimeter (DSC, Stearam Sensys), and the gas concentrations were measured using a mass spectrometer (MS, Hiden Analytica HPR 20). The total volumetric flowrate during the entire TPO experiment was 20 mL/min, which was controlled using mass-flow controllers from Bronkhorst.

The Pd/Fe/BEA and Pd/La/BEA samples were also characterized using STEM-EDX. In these measurements, powder samples of Pd/Fe/BEA and Pd/La/BEA were dispersed with iso-propanol onto a copper grid covered with a carbon film from Ted Pella (USA). EDX images were collected using an FEI Titan 20–300 instrument, and the TEM/STEM instrument was operated at 300kV. STEM imaging was performed using a high-angle annular dark-field (HAADF) detector.

In order to evaluate the oxidation state of Pd in the Pd/BEA, Pd/Fe/BEA, and Pd/La/BEA samples, X-ray photoelectron spectroscopy was used. The instrument used for the measurements was a PHI 5500 Multi-Techniques ESCA system with monochromated Al X-ray (E = 1486.6 eV) as the X-ray source. To compensate for charging effects, the spectra were aligned with the position of the Si 2p peak located at 103.6 and the Al 2p peak located at 74.8 eV, which corresponds to SiO_2 and Al_2O_3 present in the zeolite beta structure, respectively. Limitation of the measurements is for low atomic percentages in samples. For these samples, the Pd content is lower than 1 atomic percentage, which gives a level of uncertainty to the results.

3.3. Temperature-Programmed Desorption

For all temperature-programmed desorption experiments, samples coated onto cordierite monoliths were used. The reason for using monoliths in flow reactors is to acquire a more realistic flow pattern that is also more convenient for the type of instrumental setup used. The coated monolith samples were wrapped in quartz wool and placed inside a quartz tube (22 mm in diameter and 750 mm in length). The quartz tube was placed in a heating coil, and two thermocouples were used for temperature control. One thermocouple measured the temperature inside the monolith sample, and the other measured the gas temperature in front of the sample. The quartz tube was then covered in insolation. The volumetric flow of gases was controlled using mass-flow controllers and a CEM system from Bronkhorst, and the gases were measured using an MKS Multigas 2030 FTIR spectrometer.

All samples were first degreened in 10 vol % O_2 and 5 vol % H_2O at 600 °C for 2 h. Thereafter, the samples were cooled to 80 °C in 10 vol % O_2. After the degreening, four different TPD experiments were performed with oxidation in 10 vol % O_2 at 500 °C for 20 min in between each experiment. During the hydrocarbon exposure phase, the samples were either exposed to 1000 ppm toluene or 1000 ppm propene at 80 °C for 1 h. Thereafter, the samples were flushed for 20 minutes in Ar followed by a heating ramp from 80 to 500 °C with a heating rate of 20 °C/min. Dry TPD experiments were performed before wet TPD experiments, and wet TPD experiments were identical to the dry experiments with the difference that 5 vol % H_2O was present during the hydrocarbon exposure and the subsequent heating ramp.

3.4. In Situ DRIFT Spectroscopy

All monolith samples were first oxidized in 10% O_2 at a flowrate of 600 mL/min at 400 °C for 20 min, then cooled to 80 °C in the presence of oxygen. Subsequently, each sample was exposed to 500 ppm

toluene at 80 °C for 60 min, followed by an Ar-flush for 10 min. Thereafter, each sample was cooled to room temperature. This was performed in the same flow reactor setup as for the TPD experiments. After the monolith samples had been exposed to toluene, the washcoat was scraped off the coated monolith samples and used for the in situ DRIFTS experiments. In the DRIFTS experiments, the temperature was increased in steps from 80 to 350 °C at a heating rate of 10 °C/min between each step. Data on the surface species were collected every 50 °C step. This was followed by oxidation at 400 °C in 10% O_2 for 20 min. The oxidized sample, likely free from any residual hydrocarbons, was thereafter used to get background spectra that were subtracted from the other spectra. The instrument used for the DRIFTS experiments was a VERTEX 70 spectrometer (Bruker) equipped with a liquid-nitrogen-cooled mercury cadmium telluride detector, a Praying Mantis™ diffuse reflectance accessory, and a stainless-steel reaction chamber (Harrick Scientific Products Inc.). Spectra were measured between 4000–500cm^{-1} with a resolution of 4 cm^{-1}.

4. Conclusions

In this work, we have studied the effects and potential benefits of adding La and Fe to a Pd/BEA-based HC-trap system. The effect was evaluated using ethene- and toluene-TPD, in-situ DRIFTS, TPO, XPS, and STEM-EDX techniques. From the ethene- and toluene-TPD experiments, we could observe that smaller alkenes are more affected by the presence of H_2O in the feed than toluene, which appears to be negligibly affected by H_2O. Cracking effects were also observed to be inhibited by the presence of H_2O. This is most likely connected to water blocking the Brønsted acid sites, which would inhibit the cracking and polymerization of the hydrocarbons in the zeolite framework. While the addition of Fe did not show any major effect in contrast to BEA during the HC-TPD, the addition of La resulted in both an increase in the storage of toluene and an increase in the desorption temperature for toluene in wet conditions, which is beneficial.

The results from the DRIFTS experiments indicate that the addition of Pd and La provides new storage sites for toluene, and that the sites become active in the same temperature region in which toluene desorbs from zeolite beta. EDX images of agglomerated Pd particles showed that Pd and La, as well as Pd and Fe, were located in close connection, although the connection was the strongest for Pd and La. Also, TPO and XPS experiments verified an interaction between Fe/La and Pd.

Supplementary Materials: The following are available online at http://www.mdpi.com/2073-4344/10/2/173/s1, Figure S1: DRIFTS spectra during dry-toluene-TPD experiments. A stepwise measurement from 100–300 °C with only argon present in the gas feed. Panels C, G and K show the wavenumber region 4000–2000 cm^{-1}. Panels D, H and L show the wavenumber region 2000–1000 cm^{-1}.

Author Contributions: R.J., L.O. and M.S. conceived and designed the experiments; R.J. performed the experiments (except STEM-EDX); J.W. performed the STEM-EDX; R.J., J.W., M.S., and L.O. analyzed the data; R.J. wrote the paper. All authors have read and agreed to the published version of the manuscript.

Acknowledgments: The Competence Centre for Catalysis is hosted by Chalmers University of Technology and financially supported by the Swedish Energy Agency and the member companies AB Volvo, ECAPS AB, Johnson Matthey AB, Preem AB, Scania CV AB, Umicore Denmark ApS, and Volvo Car Corporation AB.

Conflicts of Interest: The authors declare no conflict of interest.

References

1. Park, J.H.; Park, S.J.; Nam, I.S.; Yeo, G.K.; Kil, J.K.; Youn, Y.K. A fast and quantitative assay for developing zeolite-type hydrocarbon trap catalyst. *Microporous Mesoporous Mater.* **2007**, *101*, 264–270. [CrossRef]
2. Kim, M.Y.; Kyriakidou, E.A.; Choi, J.S.; Toops, T.J.; Binder, A.J.; Thomas, C.; Parks, J.E.; Schwartz, V.; Chen, J.; Hensley, D.K. Enhancing low-temperature activity and durability of Pd-based diesel oxidation catalysts using ZrO_2 supports. *Appl. Catal. B Environ.* **2016**, *187*, 181–194. [CrossRef]

3. Du, S.; Tang, W.; Guo, Y.; Binder, A.; Kyriakidou, E.A.; Toops, T.J.; Wang, S.; Ren, Z.; Hoang, S.; Gao, P.X. Understanding low temperature oxidation activity of nanoarray-based monolithic catalysts: From performance observation to structural and chemical insights. *Emiss. Control Sci. Technol.* **2017**, *3*, 18–36. [CrossRef]
4. Hazlett, M.J.; Epling, W.S. Spatially resolving CO and C_3H_6 oxidation reactions in a Pt/Al_2O_3 model oxidation catalyst. *Catal. Today* **2016**, *267*, 157–166. [CrossRef]
5. Lee, J.; Theis, J.R.; Kyriakidou, E.A. Vehicle emissions trapping materials: Successes, challenges, and the path forward. *Appl. Catal. B Environ.* **2019**, *243*, 397–414. [CrossRef]
6. Wesson, P.J.; Snurr, R.Q. Modified temperature programmed desorption evaluation of hydrocarbon trapping by CsMOR zeolite under cold start conditions. *Microporous Mesoporous Mater.* **2009**, *125*, 35–38. [CrossRef]
7. Yoshimoto, R.; Hara, K.; Okumura, K.; Katada, N.; Niwa, M. Analysis of toluene adsorption on na-form zeolite with a temperature-programmed desorption method. *J. Phys. Chem. C* **2007**, *111*, 1474–1479. [CrossRef]
8. Kanazawa, T. Development of hydrocarbon adsorbents, oxygen storage materials for three-way catalysts and NOx storage-reduction catalyst. *Catal. Today* **2004**, *96*, 171–177. [CrossRef]
9. De Moor, B.A.; Reyniers, M.F.; Gobin, O.C.; Lercher, J.A.; Marin, G.B. Adsorption of C2−C8 *n*-Alkanes in Zeolites. *J. Phys. Chem. C* **2011**, *115*, 1204–1219. [CrossRef]
10. Sarshar, Z.; Zahedi-Niaki, M.H.; Huang, Q.; Eić, M.; Kaliaguine, S. MTW zeolites for reducing cold-start emissions of automotive exhaust. *Appl. Catal. B Environ.* **2009**, *87*, 37–45. [CrossRef]
11. Daldoul, I.; Auger, S.; Picard, P.; Nohair, B.; Kaliaguine, S. Effect of temperature Ramp on hydrocarbon desorption profiles from zeolite ZSM-12. *Can. J. Chem. Eng.* **2016**, *94*, 931–937. [CrossRef]
12. Dorner, R.W.; Deifalla, M.; Catlow, C.R.A.; Corà, F.; Elangovan, S.P.; Okubo, T.; Sankar, G. Heteroatom-substituted microporous AFI and ATS structured materials for hydrocarbon trap: An insight into the aluminophosphate framework-toluene interaction. *J. Phys. Chem. C* **2008**, *112*, 4187–4194. [CrossRef]
13. Li, Y.; Wang, Y.; Liu, X.; Li, X.; Pan, R.; Han, P.; Dou, T. Synthesis of hierarchical mesoporous zeolites based on MOR zeolite: Application in the automobile tailpipe hydrocarbon trap. *J. Porous Mater.* **2015**, *22*, 807–815. [CrossRef]
14. Puértolas, B.; García-Andújar, L.; García, T.; Navarro, M.V.; Mitchell, S.; Pérez-Ramírez, J. Bifunctional Cu/H-ZSM-5 zeolite with hierarchical porosity for hydrocarbon abatement under cold-start conditions. *Appl. Catal. B Environ.* **2014**, *154–155*, 161–170.
15. Nakagawa, S.; Minowa, T.; Katogi, K.; Higashiyama, K.; Nagano, M.; Hamada, I. A New Catalyzed Hydrocarbon Trap Control System for ULEV/SULEV Standard. *SAE Tech. Pap.* **2003**, 2003-01-0567. [CrossRef]
16. López, J.M.; Navarro, M.V.; García, T.; Murillo, R.; Mastral, A.M.; Varela-Gandía, F.J.; Lozano-Castelló, D.; Bueno-López, A.; Cazorla-Amorós, D. Screening of different zeolites and silicoaluminophosphates for the retention of propene under cold start conditions. *Microporous Mesoporous Mater.* **2010**, *130*, 239–247. [CrossRef]
17. Yoda, E.; Kondo, J.N.; Domen, K. Detailed process of adsorption of alkanes and alkenes on zeolites. *J. Phys. Chem. B* **2005**, *109*, 1464–1472. [CrossRef]
18. Westermann, A.; Azambre, B.; Finqueneisel, G.; Da Costa, P.; Can, F. Evolution of unburnt hydrocarbons under "cold-start" conditions from adsorption/desorption to conversion: On the screening of zeolitic materials. *Appl. Catal. B Environ.* **2014**, *158–159*, 48–59. [CrossRef]
19. Westermann, A.; Azambre, B.; Chebbi, M.; Koch, A. Modification of y Faujasite zeolites for the trapping and elimination of a propene-toluene-decane mixture in the context of cold-start. *Microporous Mesoporous Mater.* **2016**, *230*, 76–88. [CrossRef]
20. Azambre, B.; Westermann, A.; Finqueneisel, G.; Can, F.; Comparot, J.D. Adsorption and desorption of a model hydrocarbon mixture over HY zeolite under dry and wet conditions. *J. Phys. Chem. C* **2015**, *119*, 315–331. [CrossRef]
21. Burke, N.R.; Trimm, D.L.; Howe, R.F. The effect of silica:alumina ratio and hydrothermal ageing on the adsorption characteristics of BEA zeolites for cold start emission control. *Appl. Catal. B Environ.* **2003**, *46*, 97–104. [CrossRef]
22. Park, J.H.; Park, S.J.; Ahn, H.A.; Nam, I.S.; Yeo, G.K.; Kil, J.K.; Youn, Y.K. Promising zeolite-type hydrocarbon trap catalyst by a knowledge-based combinatorial approach. *Microporous Mesoporous Mater.* **2009**, *117*, 178–184. [CrossRef]

23. Liu, X.; Lampert, J.K.; Arendarskiia, D.A.; Farrauto, R.J. FT-IR spectroscopic studies of hydrocarbon trapping in Ag+-ZSM-5 for gasoline engines under cold-start conditions. *Appl. Catal. B Environ.* **2001**, *35*, 125–136. [CrossRef]
24. Kang, S.B.; Kalamaras, C.; Balakotaiah, V.; Epling, W. Hydrocarbon Trapping over Ag-Beta Zeolite for Cold-Start Emission Control. *Catal. Lett.* **2017**, *147*, 1355–1362. [CrossRef]
25. Takamitsu, Y.; Ariga, K.; Yoshida, S.; Ogawa, H.; Sano, T. Adsorption of toluene on alkali metal ion-exchanged zsm-5 and β-zeolites under humid conditions. *Bull. Chem. Soc. Jpn.* **2012**, *85*, 869–876. [CrossRef]
26. Serra, R.M.; Miró, E.E.; Bolcatto, P.; Boix, A.V. Experimental and theoretical studies about the adsorption of toluene on ZSM5 and mordenite zeolites modified with Cs. *Microporous Mesoporous Mater.* **2012**, *147*, 17–29. [CrossRef]
27. Choudhary, V.R.; Srinivasan, K.R.; Singh, A.P. Temperature-programmed desorption of aromatic hydrocarbons on silicalite-I and ZSM-5-type zeolites. *Zeolites* **1990**, *10*, 16–20. [CrossRef]
28. Kobatake, Y.; Momma, K.; Elangovan, S.P.; Itabashi, K.; Okubo, T.; Ogura, M. "Super Hydrocarbon Reformer Trap" for the Complete Oxidation of Toluene Using Iron-Exchanged β-Zeolite with a Low Silicon/Aluminum Ratio. *ChemCatChem* **2016**, *8*, 2516–2524. [CrossRef]
29. Xu, L.; Lupescu, J.; Cavataio, G.; Guo, K.; Jen, H. The Impacts of Pd in BEA Zeolite on Decreasing Cold-Start NMOG Emission of an E85 Fuel Vehicle. *SAE Int. J. Fuels Lubr.* **2018**, *11*, 239–246. [CrossRef]
30. Lupescu, J.; Xu, L.; Jen, H.W.; Harwell, A.; Nunan, J.; Alltizer, C.; Denison, G. A New Catalyzed HC Trap Technology that Enhances the Conversion of Gasoline Fuel Cold-Start Emissions. *SAE Int. J. Fuels Lubr.* **2018**, *11*, 411–426. [CrossRef]
31. Mihai, O.; Trandafilović, L.; Wentworth, T.; Torres, F.F.; Olsson, L. The Effect of Si/Al Ratio for Pd/BEA and Pd/SSZ-13 Used as Passive NOx Adsorbers. *Top. Catal.* **2018**, *61*, 2007–2020. [CrossRef]
32. Luo, J.; Mccabe, R.W.; Dearth, M.A.; Gorte, R.J. Transient Adsorption Studies of Automotive Hydrocarbon Traps. *AICHE J.* **2014**, *60*, 2875–2881. [CrossRef]
33. Huber, G.W.; Corma, A. Synergies between bio- and oil refineries for the production of fuels from biomass. *Angew. Chem.-Int. Ed.* **2007**, *46*, 7184–7201. [CrossRef] [PubMed]
34. Rao, K.N.; Kim, M.; Song, J.; Na, S.; Sik, H.; Heesung, H. Cold-Start Hydrocarbon Speciation and Trap Materials for Gasoline Engines. *SAE Tech. Pap.* **2018**, 2018-01-0940. [CrossRef]
35. Westermann, A.; Azambre, B. Impact of the Zeolite Structure and Acidity on the Adsorption of Unburnt Hydrocarbons Relevant to Cold Start Conditions. *J. Phys. Chem. C* **2016**, *120*, 25903–25914. [CrossRef]
36. Li, X.; Zhu, Z.; Zhao, Q.; Wang, L. Photocatalytic degradation of gaseous toluene over ZnAl2O4 prepared by different methods: A comparative study. *J. Hazard. Mater.* **2011**, *186*, 2089–2096. [CrossRef]
37. Sanati, M.; Andersson, A. DRIFT study of the oxidation and the ammoxidation of toluene over a TiO2(B)-supported vanadia catalyst. *J. Mol. Catal.* **1993**, *81*, 51–62. [CrossRef]
38. Du, J.; Qu, Z.; Dong, C.; Song, L.; Qin, Y.; Huang, N. Low-temperature abatement of toluene over Mn-Ce oxides catalysts synthesized by a modified hydrothermal approach. *Appl. Surf. Sci.* **2018**, *433*, 1025–1035. [CrossRef]
39. Nagao, M.; Suda, Y. Adsorption of Benzene, Toluene, and Chlorobenzene on Titanium Dioxide. *Langmuir* **1989**, *5*, 42–47. [CrossRef]
40. Wang, M.; Zhang, F.; Zhu, X.; Qi, Z.; Hong, B.; Ding, J.; Bao, J.; Sun, S.; Gao, C. DRIFTS evidence for facet-dependent adsorption of gaseous toluene on TiO2 with relative photocatalytic properties. *Langmuir* **2015**, *31*, 1730–1736. [CrossRef]
41. Liao, Y.; Zhang, X.; Peng, R.; Zhao, M.; Ye, D. Catalytic properties of manganese oxide polyhedra with hollow and solid morphologies in toluene removal. *Appl. Surf. Sci.* **2017**, *405*, 20–28. [CrossRef]